Optical properties and frequency upconversion fluorescence in a Tm3+ -doped alkali niobium tellurite glass

Gaël Poirier, Fabia C. Cassanjes, Cid B. de Araújo, Vladimir A. Jerez, Sidney J. L. Ribeiro, Younes Messaddeq, and Marcel Poulain

Citation: Journal of Applied Physics **93**, 3259 (2003); doi: 10.1063/1.1555674
View online: http://dx.doi.org/10.1063/1.1555674
View Table of Contents: http://scitation.aip.org/content/aip/journal/jap/93/6?ver=pdfcov
Published by the AIP Publishing

Optical properties and frequency upconversion fluorescence in a Tm^{3+} -doped alkali niobium tellurite glass

Gaël Poirier
Instituto de Química, UNESP, CP 355, CEP 14801-970, Araraquara, SP, Brazil and Laboratoire des Matériaux Photoniques, Bâtiment 10B, Campus de Beaulieu, Université de Rennes I, Rennes, France

Fabia C. Cassanjes
Instituto de Química, UNESP, CP 355, CEP 14801-970, Araraquara, SP, Brazil

Cid B. de Araújo[a] and Vladimir A. Jerez
Departamento de Física, Universidade Federal de Pernambuco, 50670-901 Recife, PE, Brazil

Sidney J. L. Ribeiro and Younes Messaddeq
Instituto de Química, UNESP, CP 355, CEP 14801-970, Araraquara, SP, Brazil

Marcel Poulain
Laboratoire des Matériaux Photoniques, Bâtiment 10B, Campus de Beaulieu, Université de Rennes I, Rennes. France

(Received 12 November 2002; accepted 3 January 2003)

Optical spectroscopic properties of Tm^{3+}-doped $60TeO_2-10GeO_2-10K_2O-10Li_2O-10Nb_2O_5$ glass are reported. The absorption spectra were obtained and radiative parameters were determined using the Judd–Ofelt theory. Characteristics of excited states were studied in two sets of experiments. Excitation at 360 nm originates a relatively narrow band emission at 450 nm attributed to transition $^1D_2 \rightarrow {}^3F_4$ of the Tm^{3+} ion with photon energy larger than the band-gap energy of the glass matrix. Excitation at 655 nm originates a frequency upconverted emission at 450 nm ($^1D_2 \rightarrow {}^3F_4$) and emission at 790 nm ($^3H_4 \rightarrow {}^3H_6$). The radiative lifetimes of levels $^1D_2$ and $^3H_4$ were measured and the differences between their experimental values and the theoretical predictions are understood as due to the contribution of energy transfer among Tm^{3+} ions. © *2003 American Institute of Physics.* [DOI: 10.1063/1.1555674]

I. INTRODUCTION

Tellurium-oxide glasses (TG) have been intensively investigated because of their special properties such as the large resistance against devitrification, the possibility to incorporate a large amount of rare-earth (RE) dopants and the high refractive index, which allow their utilization as nonlinear optical materials.[1–16] An important characteristic of these materials is the relatively low cutoff phonon energy compared with other oxide glasses such as silicate or phosphate glasses. This property has motivated a large number of experiments dedicated to the study of the optical properties of TG doped with RE ions, and thus these glasses are revealed to be strong candidates for uses in photonic devices. Much attention was given particularly to Tm^{3+} -doped TG because of the possibility of producing blue laser radiation pumping in the infrared and optical amplification.[9–11] In previous works, TG were chosen as a host to study energy transfer processes between RE ions in doubly and triply doped samples.[4,12–16]

In this work, we present spectroscopic properties of Tm^{3+} ion in alkali niobium tellurite glasses. This glass composition has been presented recently.[3] The addition of alkali and niobium oxides in the TG increases the rigidity of the vitreous network and shifts the characteristic temperatures to higher values. Raman scattering, differential scanning calorimetry, and optical spectroscopy of Nd^{3+} -doped samples were reported. Very large emission cross sections for Nd^{3+} transitions in comparison with other oxide glasses were measured, which indicates that this glass can be used for optical amplification. Efficient frequency upconversion (UC) emission in Tm^{3+}/Yb^{3+} codoped samples excited at 1064 nm has been reported.[4] High brightness emission around 800 nm was recorded besides weaker emissions in the blue and red. Studies of blue cooperative luminescence in Yb^{3+} -doped TG excited in the infrared was reported[5] and the contribution of optical phonons for the process was exploited to obtain enhancement of the upconversion process. More recently, large upconversion enhancement due to Tm^{3+} was observed in samples codoped with Nd^{3+}. [6]

In the present work with singly doped Tm^{3+} samples, the absorption spectra were used to determine the oscillator strengths of each transition and to obtain parameters such as transition probabilities, branching ratios, and excited states radiative lifetimes. The samples were excited in the ultraviolet and in the red. UC blue fluorescence and infrared emission were observed when red light was used for excitation. The fluorescence bands were investigated as well as the mechanisms involved in their emissions. Excited state lifetimes were compared to radiative lifetimes theoretically de-

[a]Author to whom correspondence should be addressed; electronic mail: cid@df.ufpe.br

termined and the differences observed, due to nonradiative relaxation processes, were analyzed.

II. EXPERIMENT

Samples with mol % compositions of $(60-x)TeO_2-10GeO_2-10K_2O-10Li_2O-10Nb_2O_5-xTm_2O_3$ were prepared through appropriate mixtures of reagent-grade TeO_2, Nb_2O_5, Li_2CO_3, K_2CO_3, GeO_2, and Tm_2O_3. The reagents were melted in gold crucibles for 30 min at approximately 800 °C in air. Liquids were quenched to room temperature in steel molds and annealing treatments were performed at temperatures near the glass transition temperature for 2 h and then cooled slowly at room temperature. Large quantities of RE ions could be incorporated in the samples which still present a good thermal stability, i.e., a high resistance against devitrification. The samples studied have the following concentrations in mol % of Tm^{3+}:ET ($x=0$); ET2 ($x=0.2$); ET4 ($x=0.4$); ET6 ($x=0.6$); ET8 ($x=0.8$); ET10 ($x=1.0$); ET15 ($x=1.5$); ET20 ($x=2.0$). They are stable against atmospheric moisture and samples with dimensions of several millimeters could be prepared.

The absorption spectra in the 300–3000 nm range were obtained using a double beam spectrophotometer. Fluorescence experiments with excitation at 360 nm was done using a spectrofluorimeter equipped with a xenon lamp of 450 W. For excitation in the 608 – 690 nm range, a Nd:YAG pumped dye laser (pulses of ≈10 ns) with DCM dissolved in DMSO (dimethyl sulfoxide) as the active medium was used. The fluorescence emission was dispersed using a 0.50 m spectrometer, with a resolution of 5 Å, coupled to a photomultiplier. The signals were recorded using a digital storage oscilloscope connected to a computer. All data were taken at room temperature.

III. RESULTS AND DISCUSSION

The absorption bands observed from the near-ultraviolet to the near-infrared spectra of RE-doped glasses are usually due to $4f-4f$ transitions and these absorptions are mainly associated with induced electric dipole transitions.[1,2] The oscillator strength P of each absorption band can be expressed as

$$P=\frac{mc^2n^2}{N\pi e^2\chi}\int \kappa(v)dv, \tag{1}$$

where m is the electron mass, c the speed of the light, N is the number of ions in a unit volume, e the electron charge, n is the refractive index of the sample, and $\int\kappa(v)dv$ is the integrated absorption coefficient. The local field factor for electric dipole transitions is given by $\chi=(n^2+2)^2/9n$. The value of $\int\kappa(v)dv$ for each absorption band can be determined from the absorption spectrum.

The oscillator strength for a given transition between two multiplets J and J' can be calculated using the Judd–Ofelt (JO) theory[17,18] and is given by

$$P=\frac{8\pi^2mv}{3h(2J+1)}\frac{(n^2+2)^2}{9n}\sum_{\lambda=2,4,6}\Omega_\lambda|\langle aJ\|U^\lambda\|bJ'\rangle|^2, \tag{2}$$

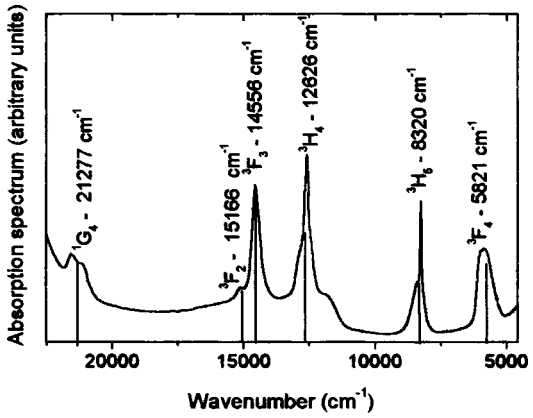

FIG. 1. Absorption spectrum at room temperture (sample ET6).

where ν is the mean frequency between the two multiplets (in cm^{-1}), U^λ ($\lambda=2,4,6$) are unit tensor operators of rank λ, and Ω_λ are the JO intensity parameters. The terms $\langle aJ\|U^\lambda\|bJ'\rangle$ are the reduced matrix elements.[19]

Equation (1) allows us to obtain the P value for each transition and these values can be used in Eq. (2) to determine the JO intensity parameters. The spontaneous radiative emission probability between J and J' levels for electric dipole transitions is given by

$$A_{JJ'}=\frac{64\pi^4v^3e^2}{3hc^3(2J+1)}\frac{n(n^2+2)^2}{9}\times\sum_{\lambda=2,4,6}\Omega_\lambda|\langle aJ\|U^\lambda\|bJ'\rangle|^2. \tag{3}$$

The radiative lifetime of an excited state is calculated by $\tau_R=(\Sigma_{J'}A_{JJ'})^{-1}$, and the branching ratio corresponding to the emission from level J to J' is given by $\beta_{JJ'}=A_{JJ'}\tau_R$. We also used the energy-gap law[20] to estimate the multiphonon relaxation rate in our samples.

Figure 1 shows the absorption spectrum corresponding to transitions from the ground state $^3H_6$ of the Tm^{3+} ion to their excited states associated to the $4f^{11}$ configuration in sample ET6. The oscillator strengths were determined from this spectrum. The obtained experimental and theoretical values of P as well as the JO parameters are presented in Table I. Changes were not observed in the line shape or in the positions of the absorption bands for different Tm^{3+} concentrations. An absorption band corresponding to the $^3H_6\rightarrow{}^1D_2$ transition does not appear in this spectrum because the energy of the $^1D_2$ level is higher than the band-gap energy of

TABLE I. Values of the experimental and theoretical oscillator strengths, and intensity parameters. $\Omega_2=3.37\times10^{-20}$ cm^2 ; $\Omega_4=1.03\times10^{-20}$ cm^2 ; and $\Omega_6=8.51\times10^{-21}$ cm^2

Transitions	ΔE (cm^{-1})	P_{EXP}	P_{THEO}
$^3H_6\rightarrow{}^3F_4$	5835	2.66×10^{-6}	2.78×10^{-6}
$^3H_6\rightarrow{}^3H_5$	8283	1.99×10^{-6}	1.69×10^{-6}
$^3H_6\rightarrow{}^3H_4$	12640	2.73×10^{-6}	2.79×10^{-6}
$^3H_6\rightarrow{}^3F_{2,3}$	14575	2.96×10^{-6}	3.06×10^{-6}
$^3H_6\rightarrow{}^1G_4$	21276	8.64×10^{-7}	8.30×10^{-7}
$^3H_6\rightarrow{}^1D_2$	28050	...	1.86×10^{-6}

TABLE II. Energy gap ΔE, transition probabilities $A_{JJ'}$, branching ratios, $\beta_{JJ'}$, between multiplets J and J' and radiative lifetime, τ_R, for each excited state

Transitions		ΔE (cm^{-1})	$A_{JJ'}$	$\beta_{JJ'}$	τ_R (ms)
$^3F_4\rightarrow$	$^3H_6$	5 821	363.84	1	2.75
$^3H_5\rightarrow$	$^3F_4$	2 499	10.08	0.03	2.80
	$^3H_6$	8 320	346.43	0.97	
$^3H_4\rightarrow$	$^3H_5$	4 306	27.84	0.01	0.50
	$^3F_4$	6 805	150.77	0.08	
	$^3H_6$	12 626	1822.90	0.91	
$^3F_3\rightarrow$	$^3H_4$	1 930	5.22	1.0 E-3	0.31
	$^3H_5$	6 236	495.76	0.15	
	$^3F_4$	8 735	84.10	0.03	
	$^3H_6$	14 556	2656.56	0.82	
$^3F_2\rightarrow$	$^3F_3$	610	0.023	1.08E-5	0.46
	$^3H_4$	2 540	23.50	0.01	
	$^3H_5$	6 846	203.02	0.09	
	$^3F_4$	9 345	1052.30	0.49	
	$^3H_6$	15 166	876.53	0.41	
$^1G_4\rightarrow$	$^3F_2$	6 111	18.12	0.01	0.33
	$^3F_3$	6 721	69.04	0.02	
	$^3H_4$	8 651	346.66	0.11	
	$^3H_5$	12 957	955.82	0.31	
	$^3F_4$	15 456	208.79	0.07	
	$^3H_6$	21 277	1449.26	0.48	
$^1D_2\rightarrow$	$^1G_4$	6 501	260.89	0.01	0.02
	$^3F_2$	12 612	1238.66	0.03	
	$^3F_3$	13 222	1671.07	0.04	
	$^3H_4$	15 152	2402.78	0.06	
	$^3H_5$	19 458	133.97	0.3E-2	
	$^3F_4$	21 957	25 314.6	0.62	
	$^3H_6$	27 778	9962.26	0.24	

the TG. However, its energy was determined performing an experiment where fluorescence in the blue region was investigated exciting the samples in the ultraviolet region as described below.

Radiative transition probabilities, branching ratios, and excited state lifetimes of all levels were determined using the JO theory and the results are presented in Table II. The errors in the calculated values were estimated as $\approx 15\%$.

Figure 2 shows the excitation spectrum of the emission at 454 nm, which was attributed to the $^1D_2\rightarrow{}^3F_4$ transition of the Tm^{3+} ion. A clear enhancement is observed when the excitation wavelength is ≈ 360 nm, indicating the energy of 27 778 cm^{-1} for level $^1D_2$. It is important to note that for this

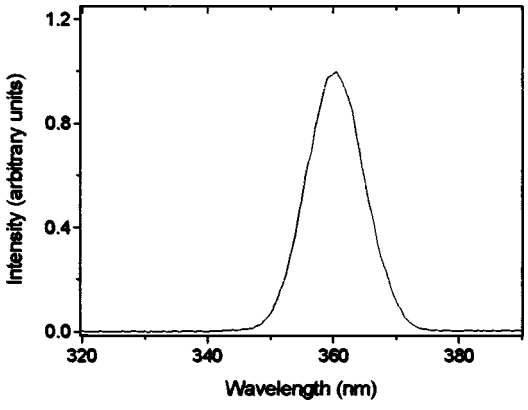

FIG. 2. Excitation spectrum of the emission at 454 nm (sample ET6).

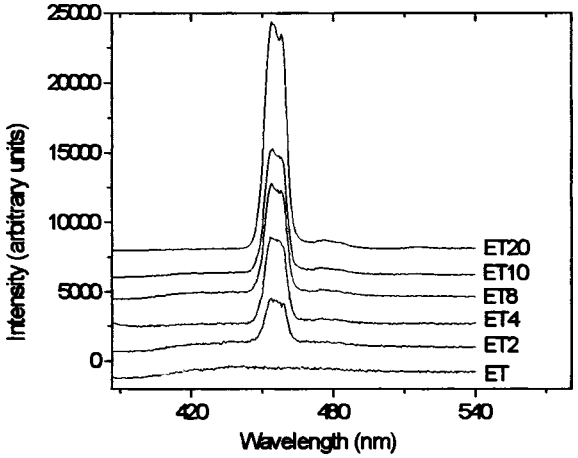

FIG. 3. Emission spectra of the glass samples for excitation at 360 nm (samples ET, ET2, ET4, ET8, ET10, and ET20). Curves were displaced in the vertical axis but were traced using the same arbitrary units.

excitation condition this is the only emission observed in the visible spectrum. This result is in good agreement with the predictions of the JO theory since the branching ratio of the $^1D_2\rightarrow{}^3F_4$ transition is about 0.62.

Emission spectra of the samples, excited at 360 nm, are presented in Fig. 3. Although the fluorescence intensities increase with Tm^{3+} concentration, we note that the samples have different sizes and thus the signal intensities cannot be directly related to the Tm^{3+} concentration. However, a linear dependence of the 450 nm emission intensity with Tm^{3+} concentration was inferred. We emphasize that the present results corroborate the interpretation given in Ref. 21 for Tm^{3+} -doped gallium lanthanum sulfide glasses where excited states of Tm^{3+} with energy larger than the energy gap of the host glass, were shown to be strongly shielded. In other words, these results show that the overlap between the 4*f* wave functions and the extended Bloch waves of the glass is small. Analogous observations were reported for Tm^{3+} -doped fluorophosphate glasses.[22]

In another experiment, the samples were excited using a pulsed dye laser operating at ≈ 655 nm (in resonance with transition $^3H_6\rightarrow{}^3F_2$) and two fluorescence bands were observed as presented in Figs. 4(a) and 4(b). To identify the mechanisms and energy pathways contributing for each emission, we investigated the dependence of the fluorescence intensity versus laser power. The results are given in Fig. 5 and the slopes of the straight lines indicate the number of absorbed laser photons for each emitted photon. The emission at ≈ 450 nm shown in Fig. 4(a) is assigned to the $^1D_2\rightarrow{}^3F_4$ transition of the Tm^{3+} ion. The quadratic dependence of the UC intensity as a function of the laser intensity indicates that a two-step one-photon absorption process (transition $^3H_6\rightarrow{}^3F_2$ followed by transition $^3F_2\rightarrow{}^1D_2$) originates the blue emission. The emission at ≈ 790 nm shown in Fig. 4(b) is due to the $^3H_4\rightarrow{}^3H_6$ transition of the Tm^{3+} ion and its excitation spectrum is presented in Fig. 6. The strong band centered at ≈ 685 nm is due to the resonant excitation of transition $^3H_6\rightarrow{}^3F_3$ with subsequent nonradiative relaxation (NRR) to level $^3H_4$ from where transition $^3H_4\rightarrow{}^3H_6$ occurs originating emission at ≈ 790 nm. The feature centered at

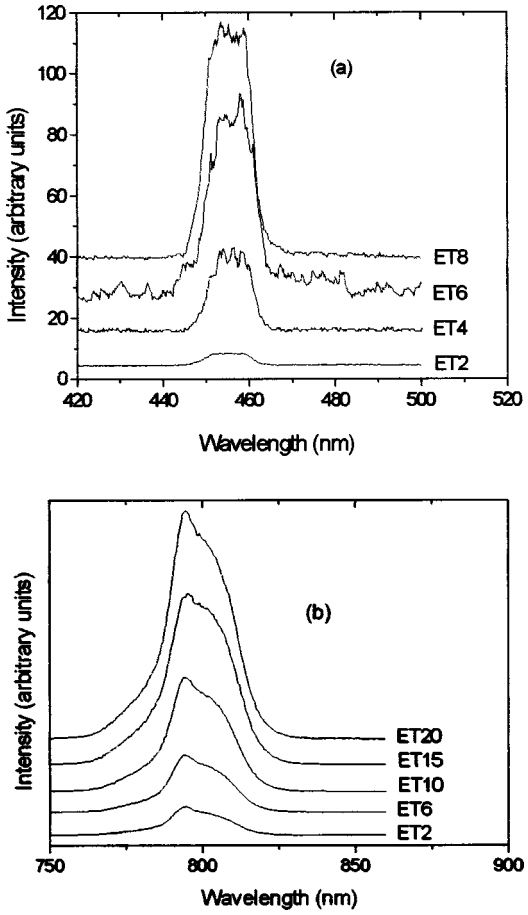

FIG. 4. (a) Upconverted emission of tellurite glasses excited at 655 nm (samples ET2, ET4, ET6, and ET8); (b) Stokes emission spectra of tellurite glasses for excitation at 655 nm (samples ET2, ET4, ET6, and ET8). Curves were displaced but were traced using the same arbitrary units.

$\approx$660 nm corresponds to the absorption to $^3F_2$ state followed by NRR to $^3H_4$ and emission at $\approx$790 nm. NRR by multiphonon relaxation (MP) from levels $^3F_{2,3}$ to $^3H_4$ is efficient because the energy gap is relatively small ($\approx$2000 cm^{-1}), which corresponds to an energy smaller than the energy of three cutoff phonons of the glass matrix.[3]

The flourescence signals centered at $\approx$450 and

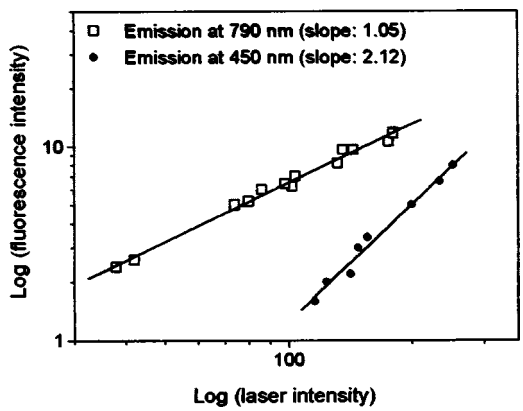

FIG. 5. Dependence between the fluorescence intensity and laser source intensity.

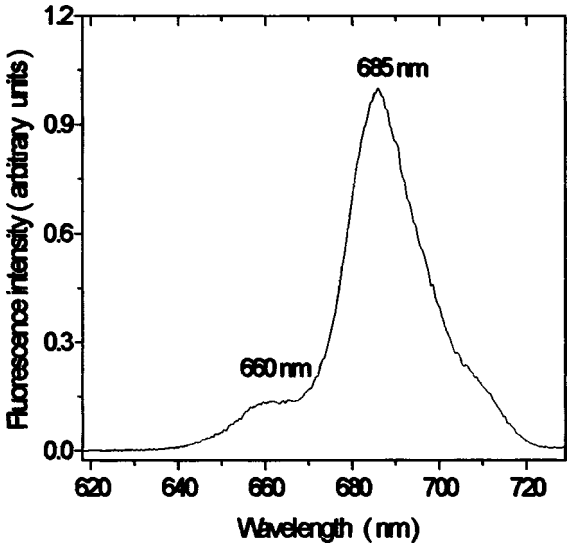

FIG. 6. Typical excitation spectrum of the emission at 790 nm (sample ET10).

$\approx$790 nm present a linear dependence as a function of Tm^{3+} concentration.

The lifetimes of $^3H_4$ and $^1D_2$ states were measured and compared with the predictions made using the JO theory. However, as shown in Table III, the measured lifetimes are different from the radiative lifetime. This indicates that nonradiative processes due to MP relaxation and/or energy transfer (ET) have to be considered. Accordingly, the excited state lifetime is described as $(\tau)^{-1}=(\tau_R)^{-1}+W_{NR}$, were τ is the actual lifetime, τ_R is the radiative lifetime calculated using the JO theory, and W_{NR} is the nonradiative relaxation rate which includes MP relaxation and ET to neighbor RE ions. The difference between τ and τ_R for the $^3H_4$ level could be due to both nonradiative processes but applying the energy-gap law[19] we estimate for the $^3H_4$ state a lifetime of $\approx$10 ms, which is about two orders of magnitude larger than the measured lifetime. This is a clear indication that MP relaxation is negligible and ET processes are playing an important role in the relaxation process for all samples. Moreover, the results in Table III indicate that W_{NR} increases for increasing values of *x*, which is expected when ET is dominant. Another indi-

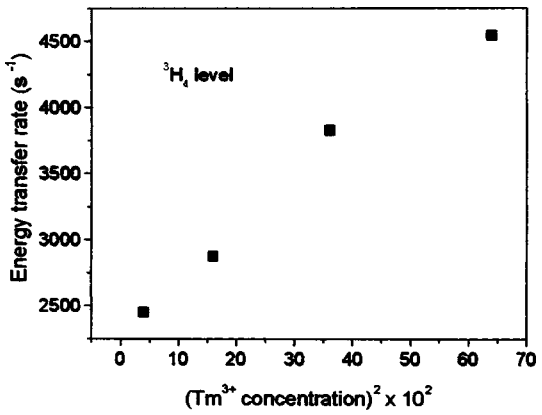

FIG. 7. Energy transfer rate for the $^3H_4$ level as a function of the Tm^{3+} concentration squared.

TABLE III. Theoretical and experimental lifetimes of $^3H_4$ and $^1D_2$ levels

	$^3H_4$ level	$^1D_2$ level
Calculated radiative lifetime	500 μs ($\pm$15%)	24 μs ($\pm$15%)
Measured lifetime		
Sample ET2 ($x=0.2$)	202$\pm$2.0 μs	3.1$\pm$2.0 μs
Sample ET4 ($x=0.4$)	186$\pm$2.0 μs	3.0$\pm$2.0 μs
Sample ET6 ($x=0.6$)	158$\pm$2.0 μs	3.0$\pm$2.0 μs
Sample ET8 ($x=0.8$)	142$\pm$2.0 μs	3.6$\pm$2.0 μs

cation that ET processes are dominant can be obtained studying the temporal decay of the fluorescence signals. The measurements did not show a single exponential decay and exhibited a time behavior typical of ET assisted processes.[23] In the case of the $^1D_2$ multiplet the measured lifetime is limited by the time resolution of the experimental system and a nonradiative relaxation rate, larger than $10^5\,s^{-1}$, can be estimated. Also in this case ET is expected to be the dominant relaxation process because the $4f$ wave functions are relatively shielded from interaction with the host matrix and the energy gap for the next Tm^{3+} level below the $^1D_2$ level is $\approx 6500\,cm^{-1}$. A possible explanation for the large ET rates is the formation of Tm^{3+} clusters and an indication of this effect is obtained plotting W_{NR} as a function of Tm^{3+} concentration, as calculated from Table III. As shown in Fig. 7, W_{NR} presents a quadratic dependence with x, but a strong nonlinear reduction in W_{NR} for $x \to 0$ indicates that the Tm^{3+} ions are not homogeneously distributed.

IV. CONCLUSION

In summary, we reported on optical spectroscopic properties of Tm^{3+} -doped tellurite glass. Physical parameters such as oscillator strengths, branching ratios between Tm^{3+} multiplets, and radiative and nonradiative relaxation rates were determined. The frequency upconversion of red light to blue light was also investigated. The results herein presented for this glass composition will be useful to support its future application in photonic devices. However, the exploitation of this system for laser operation still requires a better control of the Tm^{3+} clustering formation.

ACKNOWLEDGMENTS

The authors acknowledge financial support from Programa Nacional de Núcleos de Excelência-PRONEX/MCT (Brazil), FAPESP (Brazil), and Conseil Régional de Bretagne (France).

[1] M. Yamane and Y. Asahara, *Glasses for Photonics* (Cambridge University Press, Cambridge, U.K., 2000).
[2] *Rare-Earth-Doped Fiber Lasers and Amplifiers*, edited by M. J. F. Digonnet (Marcel Dekker, New York, 1993).
[3] F. C. Cassanjes, Y. Messaddeq, L. F. C. de Oliveira, L. C. Courrol, L. Gomes, and S. J. L. Ribeiro, J. Non-Cryst. Solids **247**, 58 (1999).
[4] P. V. dos Santos, M. V. D. Vermelho, E. A. Gouveia, M. T. de Araújo, A S. Gouveia-Neto, F. C. Cassanjes, S. J. L. Ribeiro, and Y. Messaddeq, J. Appl. Phys. **90**, 6550 (2001).
[5] P. V. dos Santos, M. V. D. Vermelho, E. A. Gouveia, M. T. de Araújo, A S. Gouveia-Neto, F. C. Cassanjes, S. J. L. Ribeiro, and Y. Messaddeq, J. Chem. Phys. **16**, 6772 (2002).
[6] N. Rakov, G. S. Maciel, M. L. Sundheimer, L. de S. Menezes, A. S. L. Gomes, Y. Messaddeq, F. C. Cassanjes, G. Poirier, and S. J. L. Ribeiro, J. Appl. Phys. **92**, 6337 (2002).
[7] K. Shioya, T. Kmatsu, H. G. Kim, R. Sato, and K. Matusita, J. Non-Cryst. Solids **189**, 16 (1995).
[8] M. J. Weber, J. D. Meyers, and D. H. Blackburn, J. Appl. Phys. **52**, 2944 (1981).
[9] W. S. Tsang, W. M. Yu, C. L. Mark, W. L. Tsui, K. H. Wong, and H. K. Hui, J. Appl. Phys. **91**, 1871 (2002).
[10] E. R. Taylor, L. N. Ng, N. P. Sessions, and H. Buerger, J. Appl. Phys. **92**, 112 (2002).
[11] M. Naftaly, S. X. Shen, and A. Jha, Appl. Opt. **39**, 4979 (2000).
[12] D. H. Cho, Y. G. Choi, and K. H. Kim, Chem. Phys. Lett. **322**, 263 (2000).
[13] S. Tanabe, T. Kouda, and T. Hanada, J. Non-Cryst. Solids **274**, 55 (2000).
[14] L. C. Courrol, L. V. G. Tarelho, and L. Gomes, J. Non-Cryst. Solids **284**, 217 (2001).
[15] D. C. Hanna, R. M. Percival, I. R. Perry, R. G. Smart, J. E. Townsend, and A. C. Tropper, Opt. Commun. **78**, 2 (1990).
[16] K. Hirao, K. Tamai, S. Tanabe, and N. Soga, J. Non-Cryst. Solids **160**, 261 (1993).
[17] B. R. Judd, Phys. Rev. **127**, 750 (1962).
[18] G. S. Ofelt, J. Chem. Phys. **37**, 511 (1962).
[19] W. T. Carnall, *Handbook of Physical Chemical Rare Earths* (North-Holland, Amsterdam, 1979).
[20] K. Tanimura, M. D. Shinn, and W. Sibley, Phys. Rev. B **30**, 2429 (1984).
[21] T. Schweizer, P. E. A Möbert, J. R. Hector, D. W. Hewak, W. S. Brocklesby, D. N. Payne, and G. Huber, Phys. Rev. Lett. **80**, 1537 (1998).
[22] K. Binnemans, R. Van Deun, C. Görller-Walrand, and J. L. Adam, J. Non-Cryst. Solids **238**, 11 (1998).
[23] M. Inokuti and F. Hirayama, J. Chem. Phys. **43**, 1978 (1965).